energies

MDPI

Article

Research on a Denoising Method of Vibration Signals Based on IMRSVD and Effective Component Selection

Xihui Chen [1,2,3,*], Xinhui Shi [1], Chang Liu [2,4] and Wei Lou [1]

[1] College of Mechanical and Electrical Engineering, Hohai University, Changzhou 213022, China
[2] School of Mechatronic Engineering, China University of Mining and Technology, Xuzhou 221116, China
[3] Engineering Research Center of Dredging Technology of Ministry of Education, Changzhou 213022, China
[4] School of Mechanical and Electrical Engineering, Xuzhou University of Technology, Xuzhou 221008, China
* Correspondence: chenxh@hhu.edu.cn; Tel.: +86-135-0614-6597

Abstract: This paper proposes a denoising method of vibration signal based on improved multiresolution singular value decomposition (IMRSVD) and effective component selection. A new construction method of trajectory matrix is used, which can enhance the oscillating component of the original signal. Next, based on the improved trajectory matrix, singular value decomposition (SVD), which plays the role of pre-decomposition, is used to obtain multiple one-dimensional components, and the further decomposition of that is achieved by multiresolution singular value decomposition (MRSVD). Finally, the effective components selection of a series of decomposed signal components is achieved based on the proposed feature evaluation index (FEI). The denoising experiments are carried out using the simulation signal and the vibration signal of planetary gear, respectively. The experimental results show that the proposed method performs better than the traditional SVD denoising method, and the weak fault feature in the vibration signal can be extracted successfully. In addition, the comparison between periodic modulation intensity (PMI) and FEI displays that the proposed method has better robustness and accuracy than the interference components with similar frequency. Thus, the proposed method is an effective weak fault feature extraction and denoising tool of vibration signals for fault diagnosis.

Keywords: denoising; vibration signal; feature extraction; IMRSVD; FEI

Citation: Chen, X.; Shi, X.; Liu, C.; Lou, W. Research on a Denoising Method of Vibration Signals Based on IMRSVD and Effective Component Selection. *Energies* **2022**, *15*, 9089. https://doi.org/10.3390/en15239089

Academic Editor: Davide Astolfi

Received: 9 October 2022
Accepted: 24 November 2022
Published: 30 November 2022

1. Introduction

Nowadays, gear is the most important transmission device in mechanical equipment, and its fault diagnosis research is of great significance to ensuring equipment safety and operation [1]. Vibration signal analysis is a widely accepted fault diagnosis tool for mechanical equipment [2]. By analyzing feature information in vibration signals, the early faults can be diagnosed while economic losses and casualties can be avoided. However, the harsh working conditions of the gear cause the vibration signal to contain a lot of noise and interference components. The fault feature information is generally covered by noise interference, and the accurate diagnosis result is hard to be gained directly [3]. Therefore, it is necessary to study the preprocessing denoising method for vibration signals which can effectively eliminate noise interference and retain fault information.

After years of development, many signal processing methods and theoretical models have been used for signal denoising and weak fault feature extraction, such as dynamic analysis [4], computational fluid dynamics [5], wavelet transform [6,7], adaptive time-frequency decomposition [8,9], blind source separation [10,11], singular value decomposition (SVD) [12], stochastic resonance [13,14], and deconvolution-based methods [15,16]. In addition, their improved methods and other sensor detection methods have also been explored and studied for better performance. Osornio-Rios [17] is based on the infrared measurement system. The classification and recognition of various faults in the transmission chain are realized through preprocessing, statistical feature extraction, high-dimensional

feature generation, and feature reduction. Zamudio-Ramirez [18] proposed a diagnosis method by analyzing stray flux signals. Statistical time domain-based features, principal component analysis, and neural networks are used to identify the uniform wear of gear. In the aspect of the vibration signal process, Hu [19] extracted the bearing fault features using a ridge extraction algorithm based on dynamic path optimization and enhanced empirical wavelet transform. The experimental results demonstrate that the proposed method is robust to noise and effective for bearing fault detection under variable speed conditions. Xiao [20] proposed a digital speckle pattern interferometry phase denoised method based on improved variational mode decomposition, which can effectively filter out noise interference. Hu [21] introduced the dual-tree complex wavelet transform into the multiscale noise tuning stochastic resonance method to improve the signal-to-noise ratio of the signal. Laha [22] proposed a modified nonlocal means denoising algorithm for the rolling element bearing fault diagnosis. The proposed method is compared with minimum entropy deconvolution, and the results show that it is robust against various noise levels.

Among the above methods, SVD is concerned and studied. SVD is a kind of matrix orthogonalization decomposition method which can effectively reflect some properties of matrices. Because of its remarkable effect in signal denoising and feature information extraction, it is applied to fault detection as well as many other fields [23,24]. Ye [25] presented a novel K times singular value decomposition-based denoising algorithm to separate the Gaussian noise from the division-of-focal-plane image and preserve the details. Yi et al. [26] proposed a quaternion singular spectrum analysis method based on convex optimization. The useful signal and noise can be distinguished by quaternion singular value decomposition to augmented trajectory matrix. Zhao et al. [27] proposed a reweighted singular value decomposition strategy. A novel information index was introduced to quantify the diagnostic information, and a truncated linear weighting function was used to control the contribution of each component during the denoised signal reconstruction. The results show that the weak fault feature with heavy noise and environmental interferences can be extracted successfully. Traditional SVD denoising can achieve good results under ideal conditions. However, in harsh working conditions, the denoising effect can be affected, and the weak fault information is easy to be lost [28,29]. These remaining problems restrict the practical application of the method, and further improvement is needed.

In this paper, a new denoising method is proposed. Combined with IMRSVD and FEI, effective signal components can be selected to reconstruct the denoising signals. The simulation and experimental results show that the proposed method performs better than the traditional SVD denoising method. The weak fault feature components in the original signal can be effectively preserved. Signal component selection is based on signal-to-noise ratio rather than signal energy. The process of decomposition and reconstruction is simple and complete, with fewer parameters to be set. These are beneficial to the practical application of the proposed method. The remainder of this paper is composed as follows: Section 2 establishes the mathematical model of the improved denoising method based on IMRSVD and FEI. In Section 3, the performance of the proposed method is tested by processing the simulation signal, and the results are compared with the traditional SVD denoising method. In Section 4, the fault signal denoising experiment is carried out, the vibration signals of the gear are processed and analyzed using the proposed method, and the effectiveness is further verified. In the last section, many conclusions are summarized.

2. Model Establishment

2.1. The Basic Theory of IMRSVD

2.1.1. The Improvement of Trajectory Matrix

The construction of the trajectory matrix is the key to the denoising method based on SVD. In this paper, a new construction method of trajectory matrix is applied. Assuming that the time series is $\{x_1, x_2, \ldots, x_N\}$, the data length is N, and the embedding dimension is set to m, the one-dimensional time series can be converted into $\boldsymbol{X} = \left\{\hat{\boldsymbol{X}}_1; \hat{\boldsymbol{X}}_2; \ldots; \hat{\boldsymbol{X}}_m\right\}$,

where $\hat{\boldsymbol{X}}_{\boldsymbol{i}} = \{\boldsymbol{x}_{\boldsymbol{i}}, \boldsymbol{x}_{\boldsymbol{i}+1}, \ldots, \boldsymbol{x}_{\boldsymbol{N}}, \boldsymbol{x}_1, \boldsymbol{x}_2, \ldots, \boldsymbol{x}_{\boldsymbol{i}-1}\}$, $\boldsymbol{i} = 1, 2, \ldots, \boldsymbol{m}$. For example, if the time series is {1, 2, 3, 4, 5, 6}, and the embedding dimension $\boldsymbol{m}$ is set as 4, then the obtained matrix is as follows:

$$\boldsymbol{X} = \begin{pmatrix} 1 & 2 & 3 & 4 & 5 & 6 \\ 2 & 3 & 4 & 5 & 6 & 1 \\ 3 & 4 & 5 & 6 & 1 & 2 \\ 4 & 5 & 6 & 1 & 2 & 3 \end{pmatrix} \tag{1}$$

Because the matrix diagonalization before SVD can enhance the oscillation components in the decomposition results of SVD, which contain more feature information and useful signals. The six elements in the lower right corner of matrix $\boldsymbol{X}$ are placed in the upper left corner to obtain the improved trajectory matrix, and it is as follows:

$$\boldsymbol{X} = \begin{pmatrix} & & & 1 & & \\ & & 1 & 2 & & \\ & 1 & 2 & 3 & & \\ 1 & 2 & 3 & 4 & 5 & 6 \\ 2 & 3 & 4 & 5 & 6 & \\ 3 & 4 & 5 & 6 & & \\ 4 & 5 & 6 & & & \end{pmatrix} \tag{2}$$

2.1.2. SVD

SVD [30] is an effective matrix analysis tool that can be used to decompose and transform a matrix. It can be used to obtain a low-rank matrix to approximate the original matrix. For the improved trajectory matrix $\boldsymbol{X}$, the existence of two orthogonal matrices, $\boldsymbol{U} \in \mathbf{R}^{m \times m}$ and $\boldsymbol{V} \in \mathbf{R}^{n \times n}$, allows the following equations to be established [31]:

$$\boldsymbol{X} = \boldsymbol{U}\boldsymbol{S}\boldsymbol{V}^{\mathrm{T}} \tag{3}$$

$$\boldsymbol{S} = \begin{bmatrix} \boldsymbol{S}_1 & O \\ O & O \end{bmatrix} \in \mathbf{R}^{m \times n} \tag{4}$$

$$\boldsymbol{S}_1 = \mathrm{diag}(\sigma_1, \sigma_2, \ldots, \sigma_r) \tag{5}$$

where $\sigma_1 \geq \sigma_2 \geq \ldots \geq \sigma_r > 0 = \sigma_{r+1} = \sigma_{r+2} = \ldots = \sigma_d$, and $\sigma_i (i = 1, 2, \ldots, \mathrm{d})$ is called the singular value of matrix $\boldsymbol{X}$, r = rank(X), and d = min(m, n).

Equation (5) is the singular value decomposition of matrix $\boldsymbol{X}$. Matrix $\boldsymbol{U}$ is the left singular matrix; matrix $\boldsymbol{V}$ is the right singular matrix. Matrix $\boldsymbol{S}$ is the singular value matrix. The SVD process of matrix $\boldsymbol{X}$ can also be represented as follows using column vectors $\boldsymbol{u}_i$ of $\boldsymbol{U}$ and column vectors $\boldsymbol{v}_i$ of $\boldsymbol{V}$:

$$\boldsymbol{X} = \sum_{i=1}^{d} \boldsymbol{u}_i \sigma_i \boldsymbol{v}_i{}^{\mathrm{T}} = \sum_{i=1}^{d} \boldsymbol{X}_i \tag{6}$$

The above equations indicate that each singular value includes the feature information of different components $\boldsymbol{X}_i$ of matrix $\boldsymbol{X}$. The large singular value indicates that the corresponding component is the main part of matrix $\boldsymbol{X}$, whereas the small singular value corresponds to the detail part.

Meanwhile, some rules must be followed during the process of reconstructing $\boldsymbol{X}_i$ into a one-dimensional component $\boldsymbol{x}_i$ of the original signal. According to the location of element $\boldsymbol{x}(t)$ in matrix $\boldsymbol{X}$, $x_i(t)$ can be obtained by calculating the mean value of the elements in the same position in $\boldsymbol{X}_i$. The specific process is as follows:

$$\boldsymbol{x}_i(t) = \overline{\boldsymbol{X}_i(a, b)} \tag{7}$$

where $t = 1, 2, \ldots, \boldsymbol{N}$, $a + b = t + 1$, $1 \leq a \leq \boldsymbol{m}$, $1 \leq b \leq \boldsymbol{n}$.

From the above, Equation (6) is equivalent to follows:

$$\boldsymbol{x} = \sum_{i=1}^{d} \boldsymbol{x}_i \tag{8}$$

Equation (8) is still established in the process of obtaining the approximate matrix of $\boldsymbol{X}$ by discarding some singular value components. This makes the signal decomposition and reconstruction using SVD only require simple addition and subtraction of one-dimensional components, which is an important basis for applying SVD in signal denoising, data compression, and other fields.

2.1.3. IMRSVD

IMRSVD uses the bisection recurrence principle for multilayers decomposition based on SVD [32], and the process of IMRSVD is as follows: Based on the construction method of improved trajectory matrix and basic SVD theory, the trajectory matrix $\boldsymbol{X}$ with embedding dimension m of the original signal $\boldsymbol{x}$ is obtained. The m matrix components $\boldsymbol{X}_1$, $\boldsymbol{X}_2$,...,$\boldsymbol{X}_\mathrm{m}$ are obtained using SVD, and m one-dimensional components $\boldsymbol{x}_1$, $\boldsymbol{x}_2$, . . . , $\boldsymbol{x}_m$ are reconstructed. This step can be called pre-decomposition. Then, for each signal component $\boldsymbol{x}_j$ (j = 1, 2, . . . , $\boldsymbol{m}$), the 2 rows trajectory matrix is constructed, and signal components $\boldsymbol{x}_j$**-1** and $\boldsymbol{x}_j$**-2** are obtained after SVD and reconstruction. The $\boldsymbol{x}_j$**-1** with a larger singular value is the main component of $\boldsymbol{x}_j$, and the $\boldsymbol{x}_j$**-2** with a smaller singular value is the detail component. Each component is decomposed in this dichotomy form, and a total of 2$\boldsymbol{m}$ components are obtained. The IMRSVD can be realized, which can be used to analyze the signal components at different scales. Meanwhile, the noise and useful features contained in the original signal will be decomposed into different signal components. The process of signal denoising can be realized by making reasonable criteria to select the useful signal components containing the feature information and reconstructing them. Figure 1 is the structure of IMRSVD.

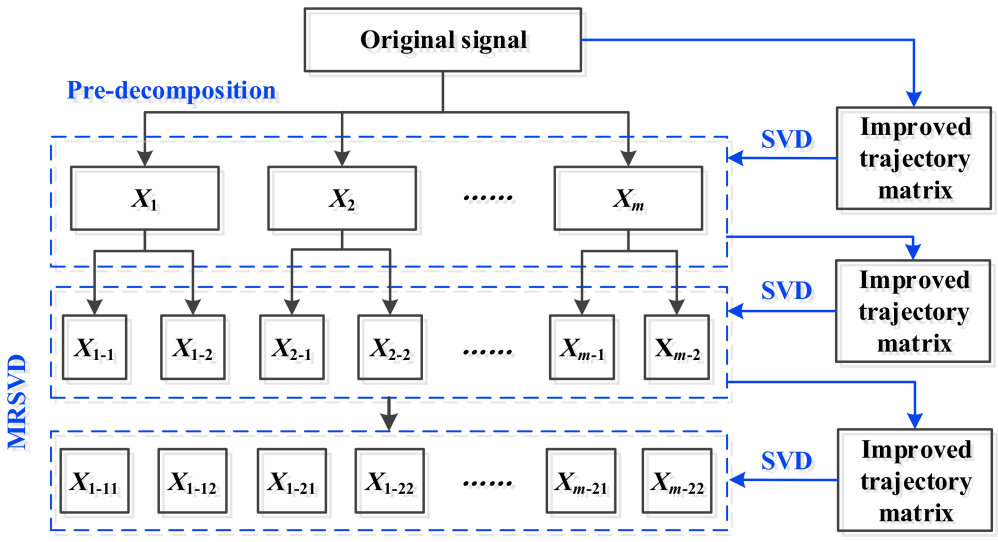

Figure 1. The structure of IMRSVD.

2.2. Effective Component Selection

In the denoising method based on traditional SVD, the larger singular values are usually selected to reconstruct the denoising signal, and the smaller singular values are zeroed. The essence of this idea is selecting signal components based on energy. However, larger energy does not mean more fault feature information. The fault feature information in the collected signal under severe working conditions is usually covered by strong noise. Even if the noise is removed, the remaining components usually include motor rotation frequency, gear meshing frequency, device resonance, and their harmonic components.

This makes selecting components based on singular values easy to ignore and discard the weak fault feature information. Therefore, a more effective component evaluation standard needs to be defined.

The envelope analysis based on the Hilbert transform can effectively detect the impulse components caused by faults. The envelope $\boldsymbol{a(t)}$ of the signal $\boldsymbol{x(t)}$ can be expressed as:

$$\boldsymbol{a(t) = abs[z(t)] = abs[x(t) + i \cdot H(x(t))]} \tag{9}$$

where $\boldsymbol{H(x(t))}$ is the Hilbert transform of the signal $\boldsymbol{x(t)}$, and $\boldsymbol{z(t)}$ is the analytic signal of $\boldsymbol{x(t)}$.

The low-frequency impact feature contained in high-frequency components can be extracted using the Hilbert envelope. Based on the above, the FEI is used to select effective components, and it is defined as:

$$\mathrm{FEI} = \boldsymbol{S}(f_0)/\boldsymbol{N}(f_0) \tag{10}$$

where $\boldsymbol{f_0}$ is the fault feature frequency. $\boldsymbol{S(f_0)}$ is the power of the envelope signal at the first $\boldsymbol{h_0}$ harmonics of $\boldsymbol{f_0}$. Generally, it is considered that the harmonic component of fault feature frequency also contains more fault feature information. If the number of harmonics selected is too small, the necessary fault feature information will be ignored. Through analysis, it is found that the signal components other than the fifth harmonic of the fault feature frequency will become very weak. Therefore, in this paper, $\boldsymbol{h_0}$ is set to 5. $\boldsymbol{N(f_0)}$ is the overall power of the envelope signal.

$\boldsymbol{S(f_0)}$ and $\boldsymbol{N(f_0)}$ can be calculated using the signal envelope spectrum. The fast Fourier transform of the signal envelope $\boldsymbol{a(t)}$ can be represented as follows:

$$\boldsymbol{A(k)} = \sum_{t=0}^{N-1} \boldsymbol{a(t)} e^{-j\frac{2\pi kt}{N}} \tag{11}$$

The sampling frequency is $\boldsymbol{f_s}$, and the frequency domain coordinates corresponding to the fault feature frequency $\boldsymbol{f_0}$ can be obtained as $k_0 = f_0(N-1)/f_s$. Thus, $\boldsymbol{S(f_0)}$ and $\boldsymbol{N(f_0)}$ can be calculated as follows:

$$\boldsymbol{S}(f_0) = \sum_{h=1}^{h_0} \sum_{i=-w}^{w} |\boldsymbol{A}(\boldsymbol{h}k_0 + \boldsymbol{i})|^2 \tag{12}$$

$$\boldsymbol{N}(f_0) = \sum_{i=0}^{N-1} |\boldsymbol{A}(\boldsymbol{i})|^2 \tag{13}$$

where $\boldsymbol{w}$ is a positive integer.

The fault gear or bearing will produce a periodic impulse feature. The frequency of impulse depends on the speed, and the strength depends on the load and fault level. The fault feature information in signal components can be effectively measured using FEI, and the fault location can be determined according to different $\boldsymbol{f_0}$. As fault feature energy is not all included in $\boldsymbol{f_0}$, the sum of the first $\boldsymbol{h_0}$ harmonics power is calculated to determine the effective component more accurately, and the interference of the periodic component with a frequency similar to $\boldsymbol{f_0}$ is reduced.

2.3. The Proposed Denoising Method

Based on the above, a denoising method based on IMRSVD and effective component selection is proposed. The flowchart of the proposed denoising method is displayed in Figure 2, and the specific steps are as follows:

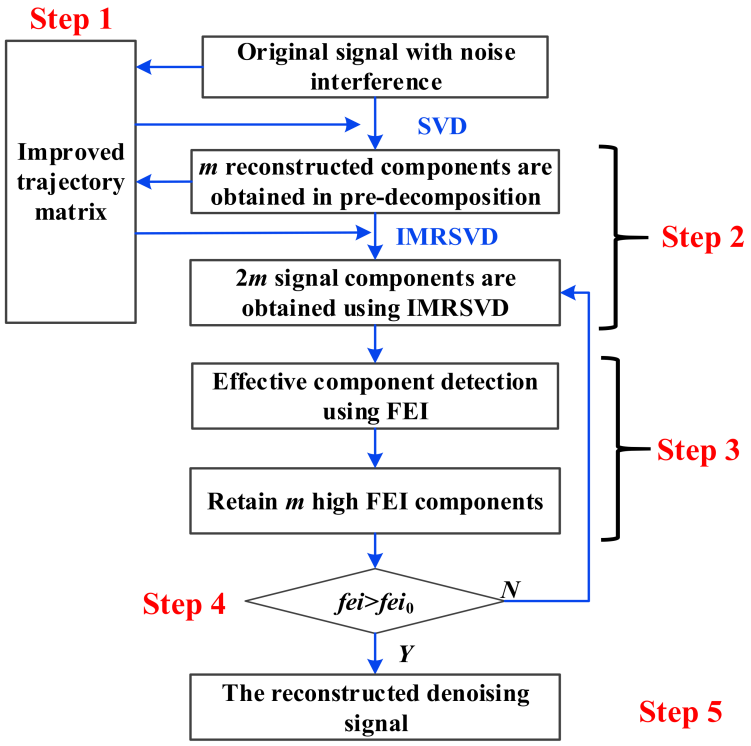

Figure 2. The flowchart of the proposed denoising method.

Step 1: The construction method of the improved trajectory matrix is established, which can enhance the oscillation components of the signal, and it is used as the basis for subsequent decomposition.

Step 2: The embedding dimension is set as $\boldsymbol{m}$, and the pre-decomposition of the original signal based on SVD is conducted, and $\boldsymbol{m}$ one-dimensional components $x_1, x_2, \ldots, x_m$ can be obtained after reconstruction. For each reconstructed component, the trajectory matrix with row 2 is further constructed, the decomposition in dichotomy form is carried out, and the main feature signal and detail feature signal corresponding to each reconstructed component can be obtained. The decomposition process of IMRSVD is realized, and a total of $2\boldsymbol{m}$ signal components are obtained.

Step 3: The FEI of $2\boldsymbol{m}$ signal components are calculated, which is used to evaluate the fault information contained in them. The fault feature frequencies $\boldsymbol{f_0}$ of different fault locations can be obtained by analyzing the transmission parameters of the equipment. The FEI of $\boldsymbol{f_0}$ can be used to evaluate the different fault feature information contained in the signal components. The $\boldsymbol{m}$ signal components with higher FEI are preserved, and the others are abandoned as noise and irrelevant signals.

Step 4: In the reserved $\boldsymbol{m}$ signal components, the maximum and minimum FEI ratio $fei = \mathrm{FEI}_{min}/\mathrm{FEI}_{max}$ is used as the index to detect, and the threshold fei_0 is set. If $fei < fei_0$, repeat step 2 to step 4 to deal with the $\boldsymbol{m}$ retained signal components from the previous round. In this process, the noise and irrelevant components in the signal can be stripped and discarded, and the effective information can be retained.

Step 5: When $fei \geq fei_0$, the iteration will be terminated. The $\boldsymbol{M}$ one-dimensional components obtained by iterative selection are reconstructed, and the final denoising signal can be reconstructed.

The setting of fei_0 is important, and if fei_0 is too large and close to 1, it means that the FEI indexes of the $\boldsymbol{m}$ reserved signal components are very similar. Since each signal component is reconstructed according to different singular values after IMRSVD, this situation is very difficult to meet, leading to too many iterations or even impossible to achieve. If fei_0 is set too small and close to 0, the iteration will be terminated quickly, and the final denoising signal still contains a lot of interference information. In this paper, through

many experiments and analyses, fei_0 is set to 0.4. The denoising process will not fall into many iterations and will not consume much time. It can also ensure that the main fault feature information is retained and has a good processing result.

3. Simulation Signal Analysis

In the actual environment, the collected vibration signal is very complex, including not only environmental noise but also multiple vibration sources inside the equipment, resulting in a low signal-to-noise ratio. In order to be closer to reality, several main sources are considered during the simulation signal construction: shaft rotation, gear meshing, fault impulse, and environmental noise. The simulation signal construction process is as follows:

$$\begin{cases} c_1 = 0.1\sin(2\times 40\pi t) \\ \quad\quad +0.05\sin(2\times 2\times 40\pi t+\pi/3) \\ \quad\quad +0.02\sin(2\times 3\times 40\pi t+\pi/3) \\ c_2 = 0.1\sin(2\times 145.83\pi t) \\ c_3 = 0.1\sin(2\times 666.67\pi t) \\ c_4 = 0.3\sum\limits_{i=1}^{\infty}\left[\sin(2000\pi(t-T(i-1)))\cdot e^{(-400abs(t-T(i-1)))}\right] \\ x_0 = c_1+c_2+c_3+c_4 \\ x = x_0+n(t) \end{cases} \tag{14}$$

where c_1 is the component of shaft rotation. c_2 and c_3 are used to simulate the components of gear meshing, and their frequencies are 666.67 Hz and 145.83 Hz, respectively. c_4 is the component of fault impulse, which is the periodic modulation of natural frequency vibration in fault position. The high-frequency vibration frequency of the simulated parts caused by impulse is 1 kHz, the impulse period is 0.048 s, and the impulse amplitude is 0.2. The simulation signal x_0 formed by these periodic vibration components can be obtained. Finally, Gauss white noise $n(t)$ is added to simulate the strong noise conditions. The signal-to-noise ratio of x_0 is adjusted to 0 dB, and the noisy simulation signal x is constructed. The sampling frequency is 10 kHz, and the sampling time is 1 s. Every signal component and the final constructed simulation signal are shown in Figure 3, and its frequency spectrums are shown in Figure 4.

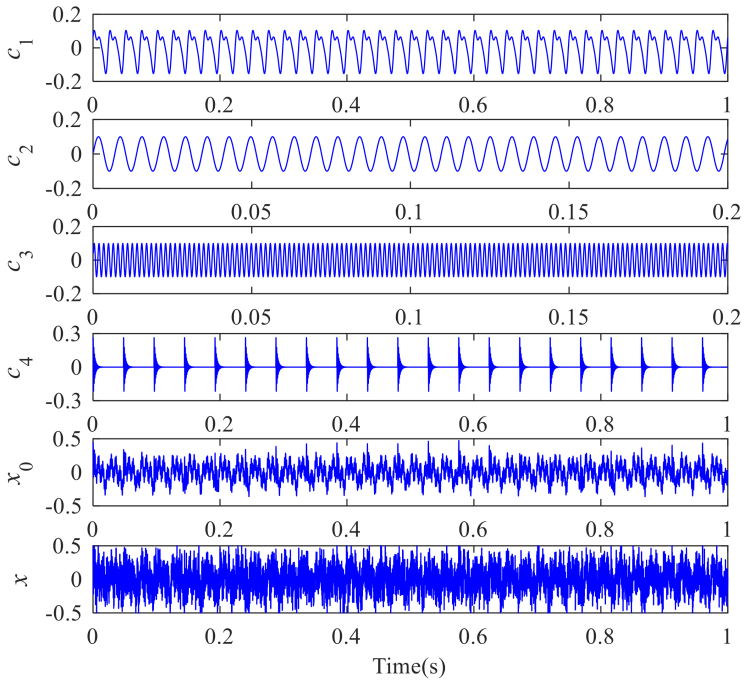

Figure 3. The final constructed simulation signal and its components.

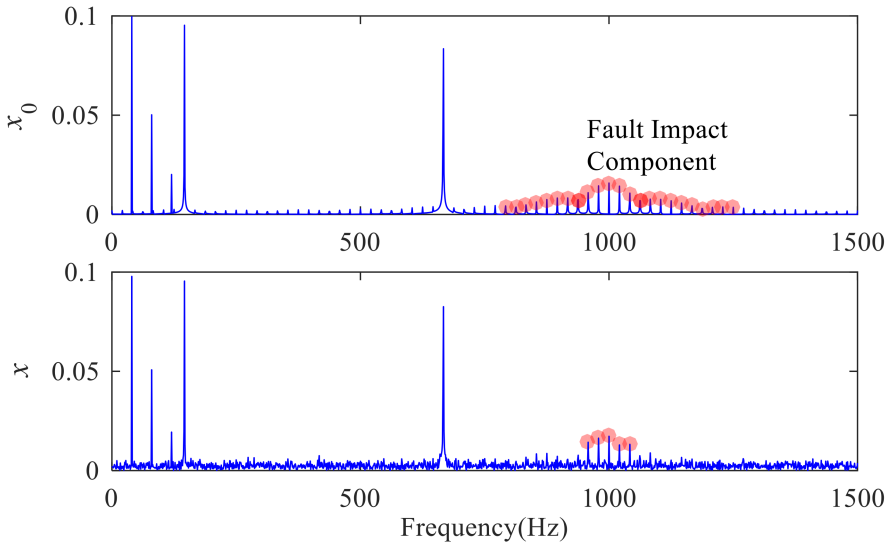

Figure 4. The frequency spectrums of the final constructed simulation signal.

It can be seen from Figures 3 and 4 that the time domain waveform of the simulation signal is regular before adding noise. The components of shaft rotation and gear meshing are obvious, while the component of fault impulse is relatively weak and difficult to be distinguished in the time domain. In the frequency domain, it distributes around the carrier frequency and is still not obvious. There is no obvious feature near the fault feature frequency. After adding Gauss white noise, the signal is submerged. In addition to strong periodic components in the spectrum, most scattered fault features are all disturbed. In Figure 5, the signal is demodulated directly using the Hilbert envelope. The envelope spectrum of simulation signal x_0 is relatively clean, but the fault feature peaks are relatively weak due to the influence of various irrelevant periodic components. The envelope spectrum of the final constructed simulation signal x' is more chaotic, and the obvious fault feature does not appear. The weak peak position does not correspond to the fault feature frequency. This means that the noise and interference components greatly influence the frequency and amplitude feature of fault components, which cannot be resolved or demodulated directly.

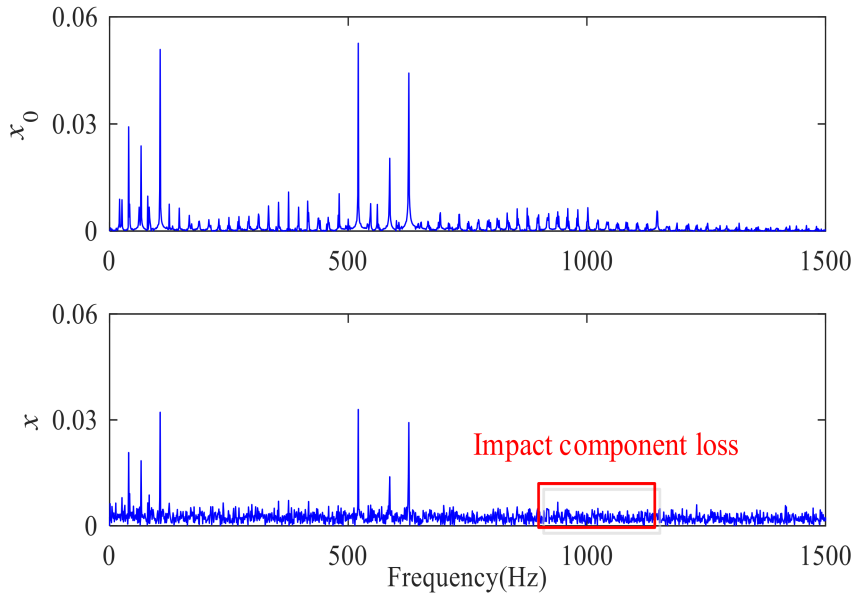

Figure 5. The envelope spectrums of the constructed simulation signal.

The denoising method based on traditional SVD is adopted to process the constructed simulation signal, and the first four components with larger singular values are used to reconstruct the denoising signal. The denoising process is displayed in Figure 6; x_1–x_6 are the first six components obtained by SVD, and $\overline{x}$ is the denoising signal obtained by reconstructing the first four components corresponding to larger singular values. The frequency spectrum and envelope spectrum of the denoising signal are shown in Figure 7, and the comparison between singular values and FEI is shown in Figure 8. The high-frequency components of the original simulation signal are weakened, and the periodicity is more obvious. In addition, it can be seen from the denoising signal in Figure 6 that no clear impulse feature appears, and the peak value corresponding to the fault feature frequency cannot be found both in the frequency spectrum and envelope spectrum. That is because the retained components are not related to the fault, while x_5 and x_6, which mainly contain impulse features, are ignored. It also can be seen from Figure 8 that x_5 and x_6 components have larger FEI values, which is the proposed index for the selection of effective components. If the retained effective components are determined according to the first four FEI values, x_5 and x_6 components containing fault impulse feature signals can be retained and reconstructed. The denoising method based on traditional SVD selects effective components according to the size of singular values, and the denoising process is based on energy instead of fault information. Under strong noise conditions, the singular values of effective components are usually small. The high threshold of singular values will result in the loss of effective components, while the low threshold will retain a large number of noise and irrelevant components. In addition, some noise is still included in the effective components after only one-time decomposition. All of these reduce the denoising effectiveness.

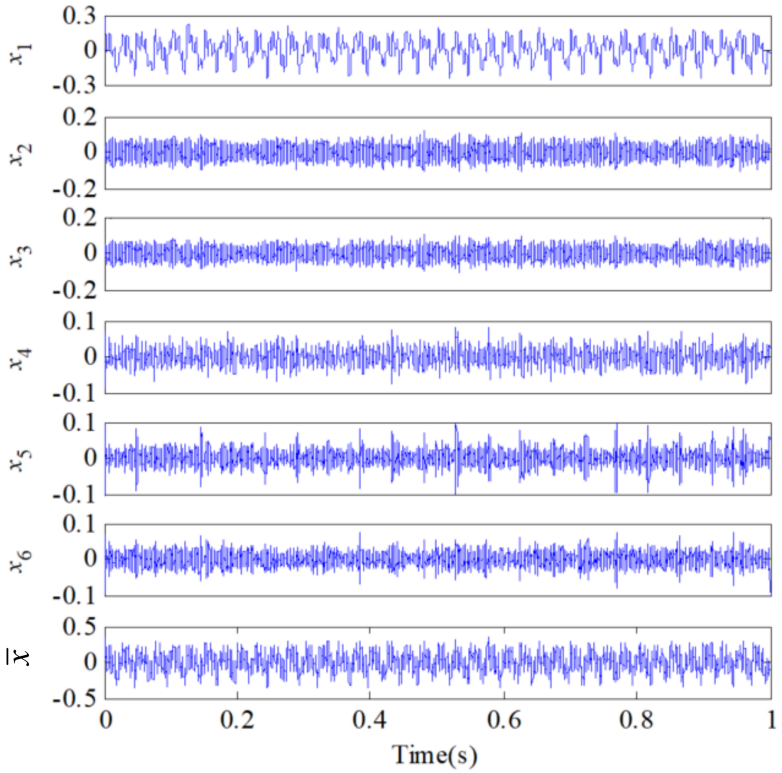

Figure 6. The denoising process based on traditional SVD and the denoising signal.

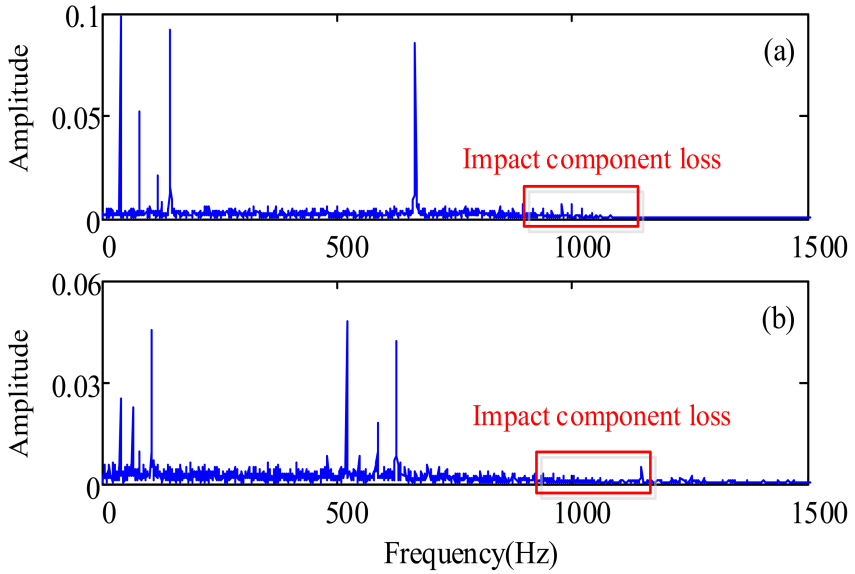

Figure 7. The frequency spectrum and envelope spectrum of the denoising signal. (**a**) frequency spectrum, (**b**) envelope spectrum.

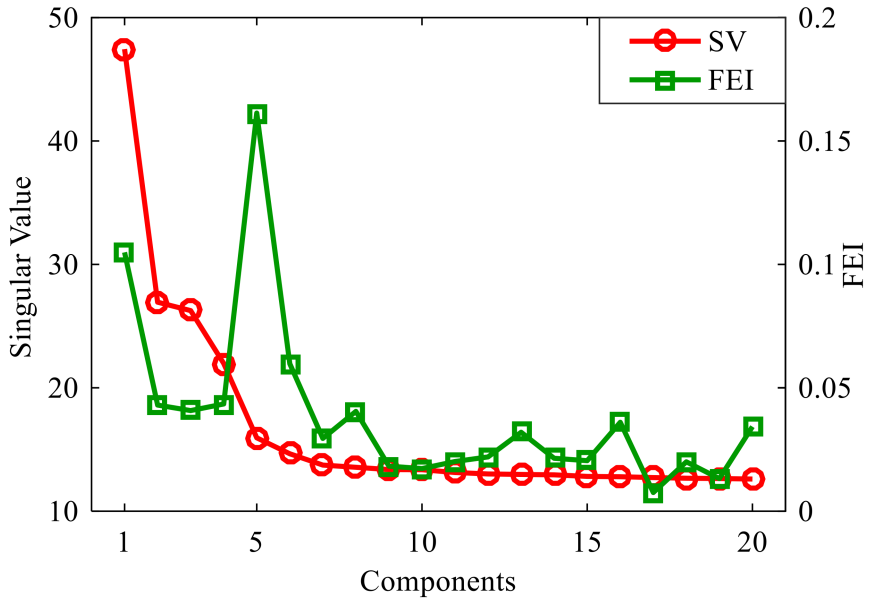

Figure 8. Comparison between singular value and FEI.

The proposed denoising method based on IMRSVD and effective component selection is used to process the simulation signal, and the denoising process and denoising results are displayed in Figures 9 and 10. The embedding dimension $\boldsymbol{m}$ is equal to 20, and the threshold $\boldsymbol{fei_0}$ is set as 0.4. The different components are preliminarily separated in the pre-decomposition stage and sorted according to singular value size. It can be seen from Figure 9 that the FEI of most components in the pre-decomposition stage is smaller, except x_1, x_5, and x_6. The FEI of x_5 and x_6 with impulse features is 0.2 and 0.08, respectively, while that of x_1 is 0.1, which mainly contains irrelevant periodic components. The sequences of effective components with obvious fault features are relatively backward. Using IMRSVD for further processing, the components with low FEI are gradually eliminated, and the whole FEI level of the retained components is gradually increased.

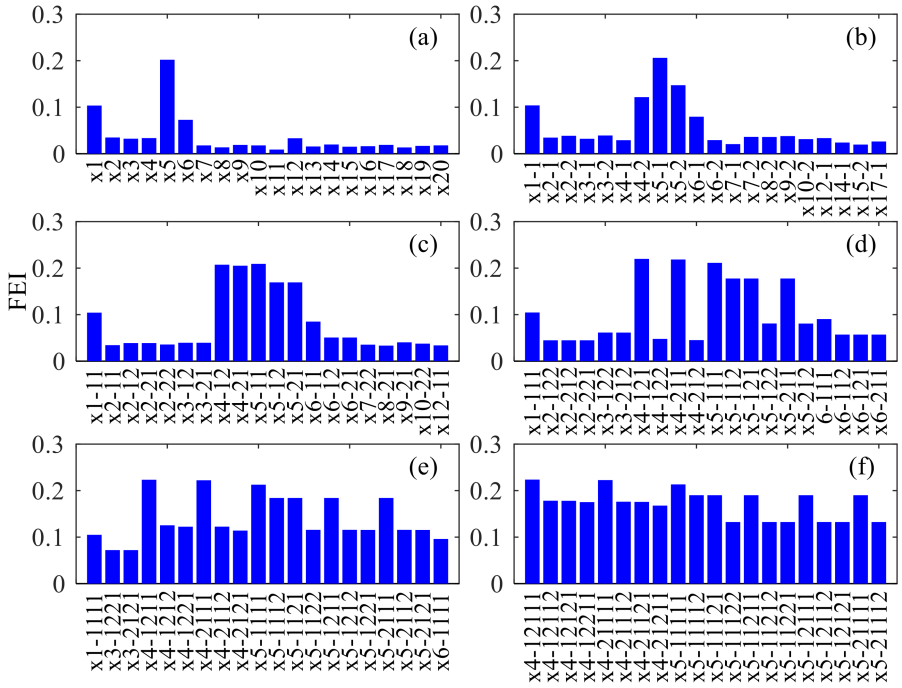

Figure 9. Improved SVD denoising method process: (**a**) pre-decomposition, (**b**) 1st MRSVD, (**c**) 2nd MRSVD, (**d**) 3rd MRSVD, (**e**) 4th MRSVD, and (**f**) 5th MRSVD.

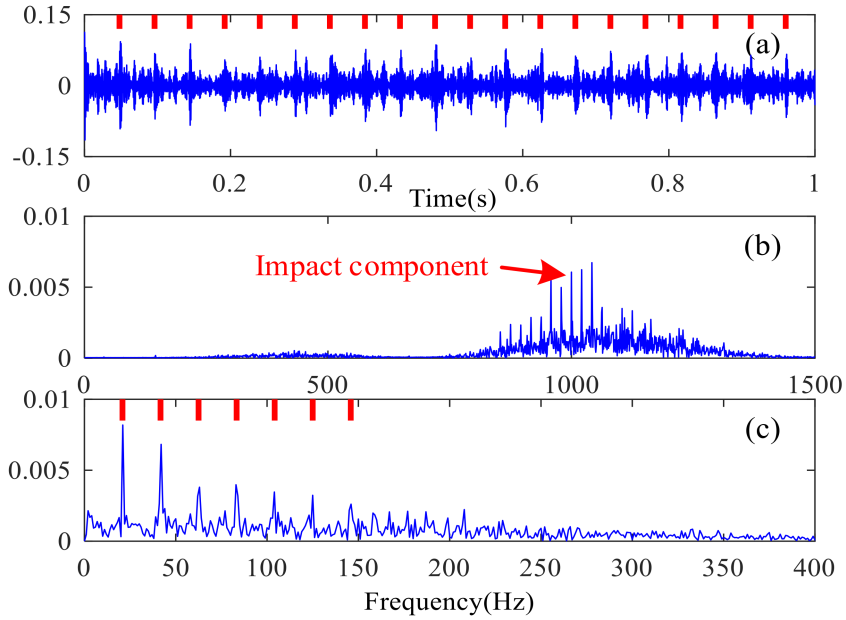

Figure 10. Denoising results: (**a**) reconstructed signal, (**b**) frequency spectrum, and (**c**) envelope spectrum.

The main components of the final retention are mainly from x_4 and x_5 in the pre-decomposition stage, and the whole FEI level is above 0.185. It should be noted that the FEI of x_4 is low, which indicates that the proposed method can detect and extract weak fault impulse components. For the obtained denoising signal in Figure 10, the impulse features caused by the fault are obvious in the time domain. The impulse period is about 0.048 s, and the frequency is about 20.83 Hz, which coincides with the fault feature frequency f_0. The average amplitude of impulse is still quite large compared with the original fault component. The envelope spectrum of the denoising signal shows that the peak value at point f_0 is obvious. In addition, the denoising signal's frequency spectrum

shows that the other components are completely suppressed except for the high-frequency vibration of fault information. This indicates that the loss of fault information during the denoising process is less, and other components are effectively separated to avoid interference with diagnosis.

4. Experimental Analysis

(1) Experimental setup

The original vibration signals of the real experiment are collected on the DDS mechanical fault comprehensive simulation bench made by Spectra Quest Company from the United States. The simulation bench is displayed in Figure 11 and comprises a motor, planetary gearbox, parallel shaft gearbox, magnetic brake, data acquisition system, and laptop. The motor can be set to any output speed through the control software. The planetary gearbox has a two-stage planetary gear structure; its specific parameters are shown in Table 1. The parallel shaft gearbox has a two-stage spur gear transmission structure, and the magnetic brake provides load simulation. The data acquisition system collects the vibration signal generated by the simulation bench and transmits it to the laptop computer through the USB interface for storage and analysis. In this experimental setup, its fault usually appears due to the frequent mesh of sun gear of the planetary gearbox. Therefore, the normal sun gear and sun gear with the second stage planetary gear breakage in the planetary gearbox are simulated, and the measured sun gears are displayed in Figure 12. A triaxial sensor and several uniaxial sensors are used to collect vibration signals, and the sampling frequency is set as 10,240 Hz. The motor output frequency is set to 40 Hz, and the load is set to 13.5 N·m by a magnetic brake. The meshing frequency and fault feature frequency of the planetary gearbox can be calculated and shown in Table 1.

(2) The analysis of the proposed method

The vibration signals of different gear states can be collected on the basis of the simulation bench. The vibration signals and spectrums of normal gear and gear with breakage are displayed in Figure 13, respectively. It can be seen from Figure 13 that there is no obvious difference in vibration signals between normal signal and gear with breakage in the time domain. The vibration signal of gear with breakage has an impulse feature, but its period is not corresponding to fault feature frequency. There are a few differences in the low-frequency band in the frequency domain, and more features appear in the high-frequency band. However, the fault cannot be directly diagnosed as happening. Compared with simulation signals, the components of the collected experimental signals are more complex. The FEI of the vibration signals of the normal gear and gear with breakage are 0.028 and 0.034, respectively, which coincides with the unsatisfactory signal condition before denoising.

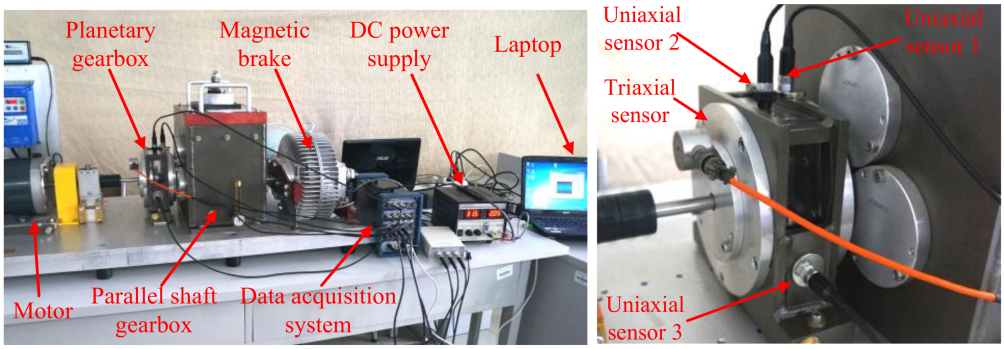

Figure 11. The simulation bench and the installation position of sensors.

Table 1. Basic parameters of two-stage planetary gearbox.

	First Stage			Second Stage		
	Sun Gear	**Planet Gear**	**Ring Gear**	**Sun Gear**	**Planet Gear**	**Ring Gear**
Number of teeth	20	40	100	28	36	100
Fault feature frequency (Hz)	100	16.67	20	20.83	4.05	5.83
Meshing frequency (Hz)		666.67			145.83	

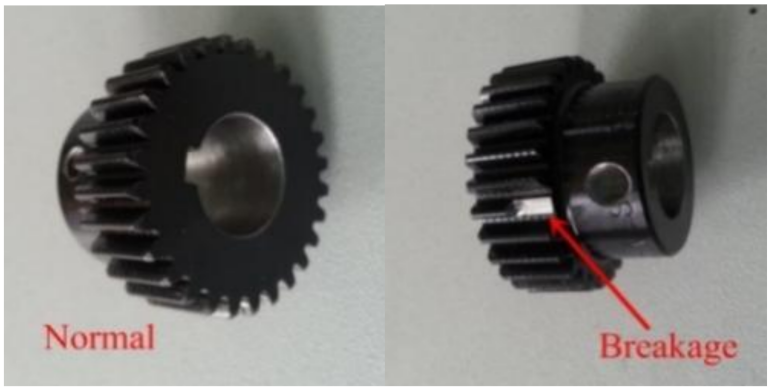

Figure 12. The measured sun gears.

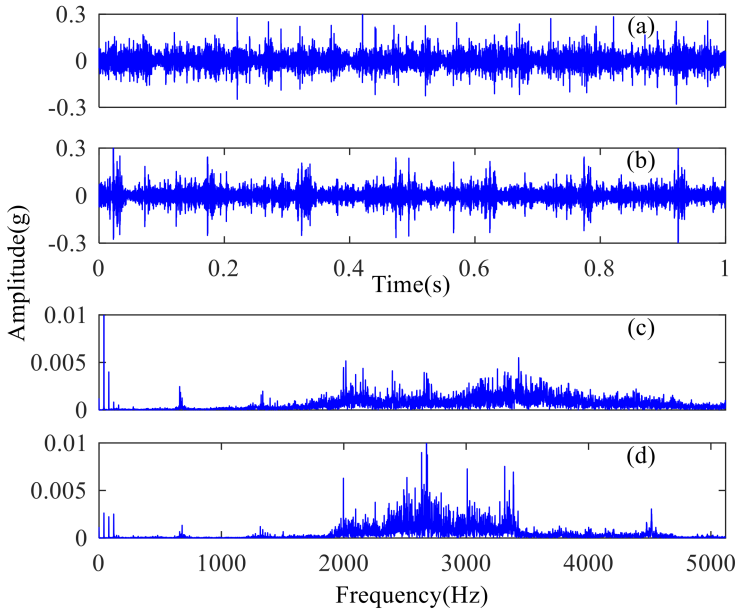

Figure 13. The vibration signals and spectrums of normal gear and gear with breakage: (**a**) vibration signal of normal gear, (**b**) vibration signal of gear with breakage, (**c**) frequency spectrum of normal gear, and (**d**) frequency spectrum of gear with breakage.

The denoising method based on traditional SVD is used to deal with the vibration signals of normal gear and gear with breakage. The first 6 components with larger singular values are selected to reconstruct the denoising signals, which are displayed in Figure 14. Compared with the original vibration signals, the denoising signals of normal gear and gear with breakage have little improvement except for a slight amplitude decrease in the time domain. The frequency spectrum shows that low-frequency interference is suppressed. Although there is a peak at f_0 in the envelope spectrum, the harmonic components do not appear. Thus, it is hard to determine if there is a fault. According to Figure 15,

the signal components corresponding to the first 6 maximum FEI values are selected for reconstruction, many interference components are still retained, and x_7, x_{16}, and x_{19} which mainly contain impact features, are abandoned. The FEI of the denoising signal of normal gear and gear with breakage are 0.032 and 0.04, respectively. That causes the loss of the fault feature information.

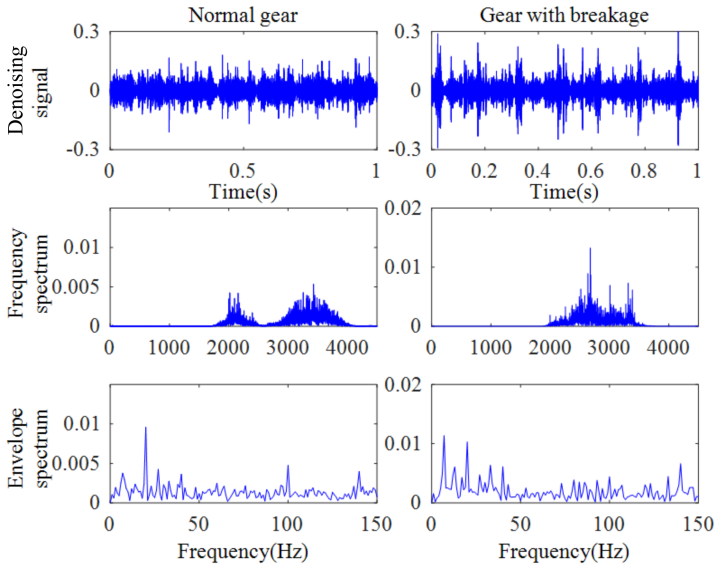

Figure 14. Denoising results based on traditional SVD.

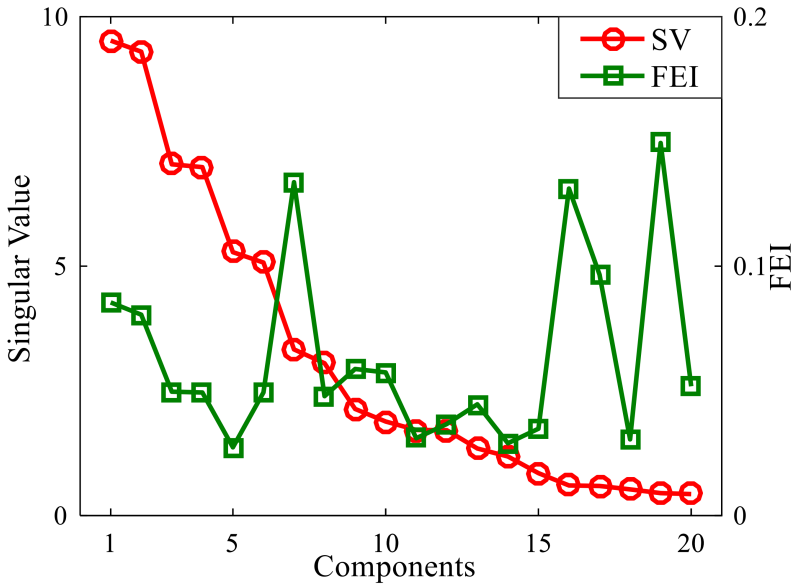

Figure 15. Comparison between singular value and FEI.

The proposed method based on IMRSVD and effective components selection is used to process the vibration signals. If the embedding dimension m is set too small, the number of signal components obtained by IMRSVD will decrease, making the fault feature information gather in a few signal components. However, the fault feature information is relatively weak. If one of the signal components is eliminated, the fault feature information may be lost. If the embedding dimension m is set too large, a large number of signal components will be obtained. The weak fault feature information may be decomposed into a large number of signal components, which also easily leads to false elimination of fault feature information. In this paper, the embedding dimension m is set to 20 through

many experiments, and the threshold fei_0 is set as 0.4. The denoising process is shown in Figures 16 and 17, and the denoising result is shown in Figure 18. For the vibration signal of gear with breakage, the iteration is stopped after three times IMRSVD. The signal components, which are independent of the fault feature, are separated gradually, and the FEI value of the obtained denoising signal is 0.125, which is higher than that obtained based on traditional SVD. Finally, the time-domain waveform of the denoising signal has a more obvious impulse feature corresponding to the fault period of 0.048 s. Although there are still some interference components in the denoising signal of gear with breakage, its envelope spectrum is cleaner and has more obvious peaks at fault feature frequency and harmonic points than that of normal gear. At the same time, the signal spectrum keeps some high-frequency characteristics, and the rest are obviously weakened. It should be noted that the periodic impulse of the signal has the characteristics with some amplitude and frequency modulation, which is related to the special structure of planetary gear.

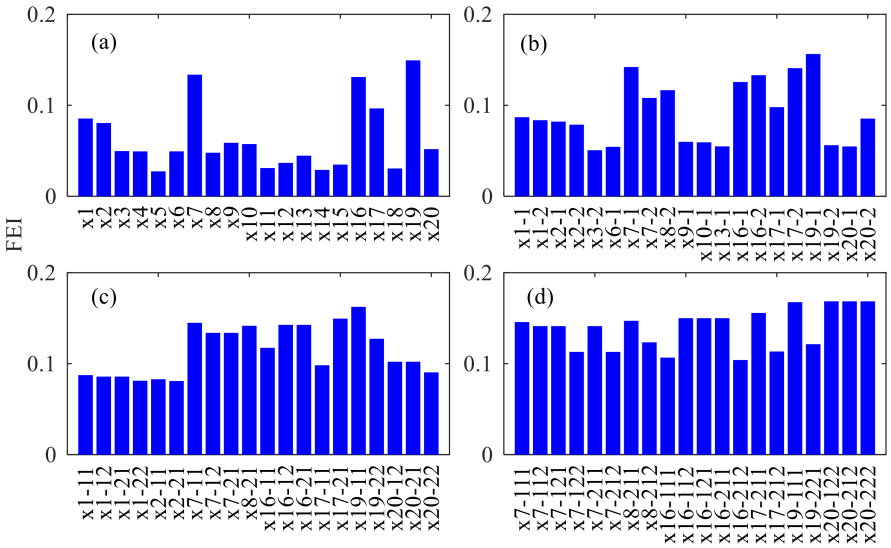

Figure 16. Denoising process based on IMRSVD for gear with breakage: (**a**) pre-decomposition, (**b**) 1st IMRSVD, (**c**) 2nd IMRSVD, and (**d**) 3rd IMRSVD.

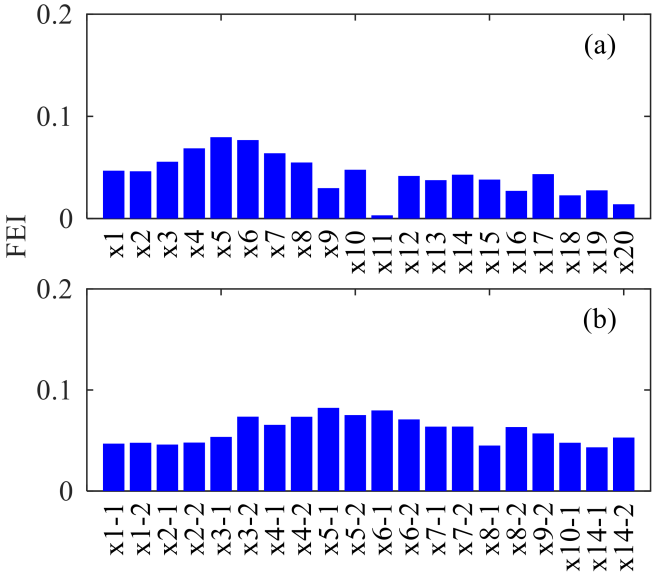

Figure 17. Denoising process based on IMRSVD for normal gear: (**a**) pre-decomposition, (**b**) 1st MRSVD.

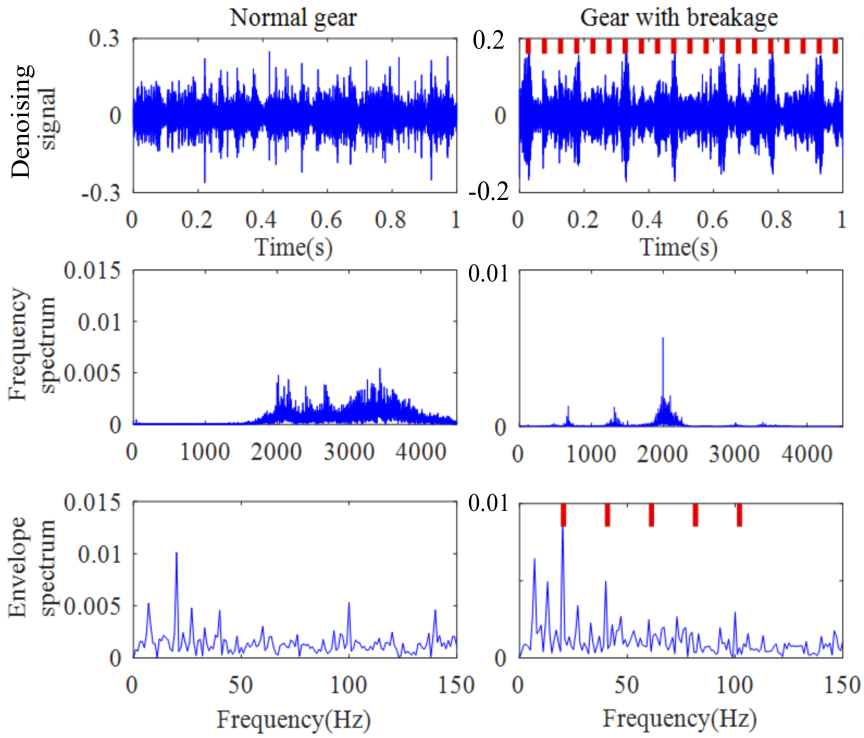

Figure 18. Denoising results based on the proposed method.

For the vibration signal of normal gear, the iteration is stopped after only one-time IMRSVD. Some irrelevant signal components are also separated, and the final denoising signal has a larger amplitude. However, the whole level of its FEI is obviously lower than that of gear with breakage, and the FEI of the denoising signal of normal gear is 0.048. There is no periodic impulse feature of denoising signal in the time domain, and the envelope spectrum has no obvious peak value at fault feature frequency. Hence, the gear can be considered to be in normal condition. In addition, although the motor rotation frequency is similar to the second harmonic of the fault, it is eliminated in the IMRSVD stage. On the one hand, FEI realizes the accurate detection and recognition of fault features. On the other hand, the multiple selections of signal components by IMRSVD can improve the signal-to-noise ratio. In order to compare the embedding dimension setting's effectiveness in the proposed method, the denoising results of gear with breakage when the embedding dimension is set to 10 and 30, respectively, are shown in Figure 19. By comparing Figures 18 and 19, it can be found that when the embedding dimension is 10, the time-domain waveform of the denoising result does not show the signal periodicity of gear with breakage. Through the analysis of its frequency spectrum, it can be seen that there are still many signal components in the frequency band greater than 4000 Hz. From its envelope spectrum, it can be found that the retained outstanding signal components are motor rotation frequency and its harmonic frequency, and the fault feature frequency information corresponding to gear with breakage has been completely eliminated, so there is no way to judge the occurrence of fault through the envelope spectrum. When the embedding dimension is 30, the time domain waveform of the denoising results shows weak periodicity, and there are many signal components in the frequency band around 3000 Hz in its spectrum. In its envelope spectrum, although the fault feature information of gear with breakage is retained, the motor rotation frequency interference is eliminated. However, the harmonic component of the fault feature frequency corresponding to the gear with breakage is also eliminated, and there is no corresponding peak value at the harmonic part.

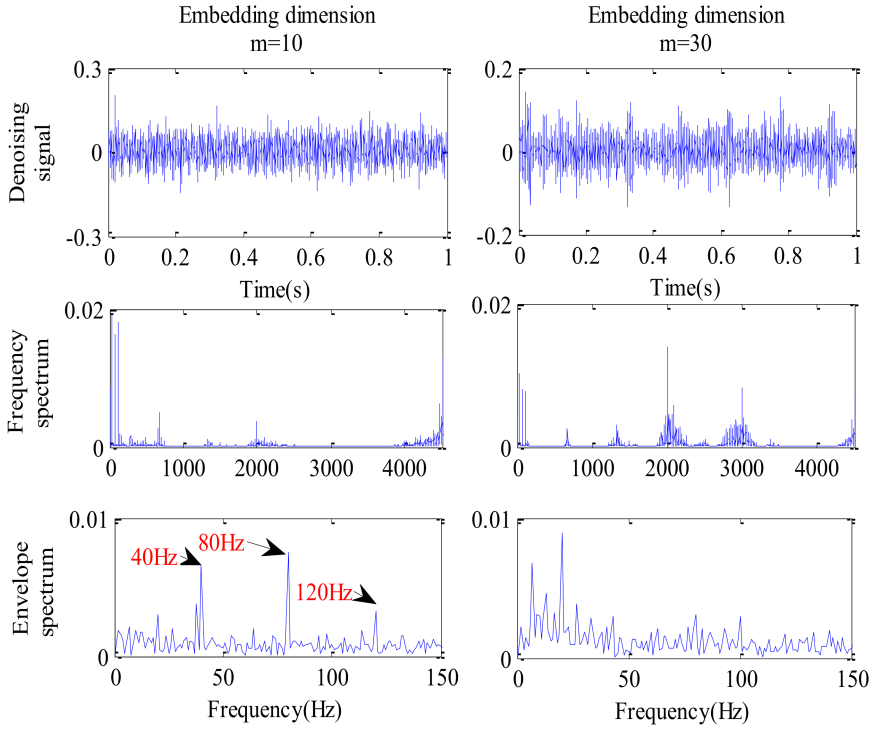

Figure 19. Denoising results of gear with breakage when embedding dimension ***m*** is set to 10 and 30, respectively.

In order to further quantitatively compare the effectiveness of the proposed method, the FEI of the original signals of normal gear and gear with breakage, the FEI of the denoising results by traditional SVD method and the FEI of the denoising results by the proposed method are compared and shown in Table 2. It can be seen from Table 2 that the FEI values of the original signals are small. After processing the traditional SVD denoising method, the FEI values increase, but the increase is not obvious. The FEI value of the fault feature frequency of gear with breakage only increases from 0.034 to 0.04. After the processing by the proposed method in this paper, the FEI value of the normal gear increases from 0.028 to 0.048. The FEI value of gear with breakage is greatly improved from 0.034 to 0.125. This means that the denoising results obtained by the proposed method contain more fault feature information. The FEI value of gear with breakage is obviously higher than that of normal gear, and the state of the gear can be judged according to the FEI value and spectrum analysis. From the above analysis, it can be seen that the proposed method can effectively extract and retain signal components containing fault information and obtain better denoising effect.

(3) Discussion

The essence of fault feature information in vibration signals is the periodic modulation caused by fault impulse. Therefore, effective component selection requires the demodulation and measurement of fault feature information. However, except for noise interference, the original vibration signal usually contains many components which are independent of the fault. They may have considerable energy, and the effective fault information can be disturbed. Envelope demodulation based on the Hilbert transform is an effective method, and SVD combined with the Hilbert transform can better separate noise and interference. As shown in Figure 20, the low-frequency impulse contained in high-frequency vibration can be displayed using an envelope.

Table 2. The comparison of FEI with different processing method.

	Original Signals		**Denoising Result by Traditional SVD**		**Denoising Result by the Proposed Method**	
Gear state	Normal	Breakage	Normal	Breakage	Normal	Breakage
FEI	0.028	0.034	0.032	0.04	0.048	0.125

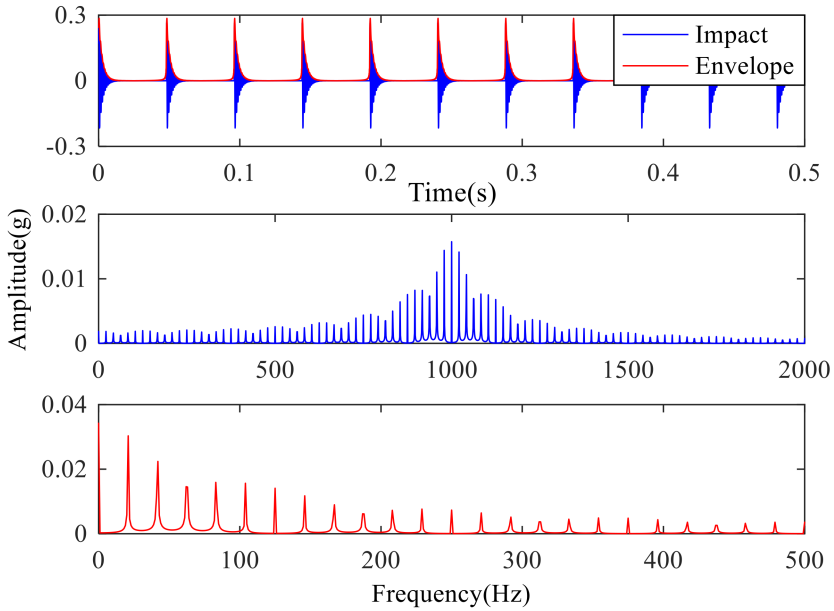

Figure 20. Envelope demodulation of fault impulse.

A reliable index that can measure fault feature information is needed to realize effective component selection. The proposed FEI is based on envelope spectrum analysis and the signal-to-noise ratio at the feature frequency f_0, which can be used to achieve effective component selection. Similarly, [27] proposed a component selection index called PMI based on autocorrelation detection, and it is shown in Equation (14):

$$\mathrm{PMI} = \frac{E_p}{E_n} = \frac{R_a(T)}{R_a(0) - R_a(T)} \tag{15}$$

where E_p and E_n are the power of periodic components and noise, respectively. R_a is the autocorrelation function of signal envelope a. T is the first peak location of R_a, i.e., the period of periodic components in envelope a. Based on the autocorrelation function, the periodic components in the signal envelope can be detected, and their contents can be calculated according to PMI. The PMI of fault feature frequency f_0 can be used to determine whether the signal component contains obvious fault feature information. However, PMI also has some problems. On the one hand, the PMI of effective components is still small due to noise interference. On the other hand, PMI has a weaker distinguishing ability on irrelevant periodic components. The envelope autocorrelation function of component x_{13} of gear with breakage and the comparison between PMI and FEI are shown in Figure 21, and it can be seen that the calculated PMI at fault impulse period T will be large enough because the motor frequency is similar to the fault feature frequency harmonics. This will interfere with the effective component selection. By comparing the FEI and PMI of gear with breakage, it can be seen that PMI gives an overestimate to motor rotation vibration. Thus, although PMI has some advantages in analyzing the pure signal, it will be affected when the signal components are complex and noisy. On the contrary, FEI shows better accuracy and robustness against these problems. It can limit the assessment scope to the fault feature frequency more accurately. As the energy of typical impulse attenuates with harmonic

sequence, FEI only takes the power sum of the first few harmonics during calculation. This both ensures effective component selection accuracy and avoids the misjudgment of other components.

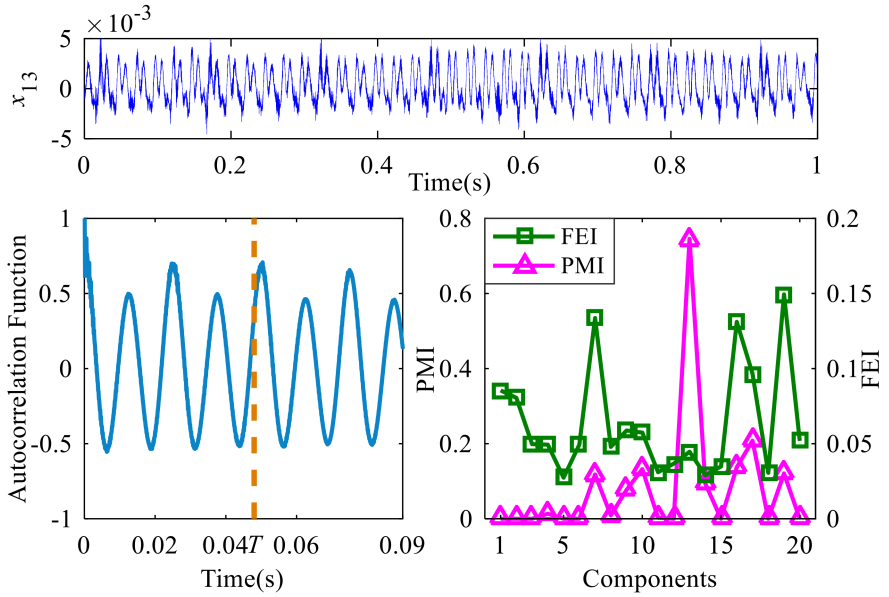

Figure 21. The autocorrelation function of component of gear with breakage and the comparison between PMI and FEI.

Based on the effective component selection using FEI, further component decomposition and selection using IMRSVD can be achieved. The components with low FEI are constantly abandoned to avoid unnecessary calculations. The components with high FEI will be further decomposed and purified during the next iteration. These improve the whole FEI level of the components left in each round of IMRSVD. As also can be seen from Figures 9 and 16, the components with high FEI at the early stage have abandoned subcomponents after further processing. This indicates that the components with high FEI still contain some interference, and the proposed method can effectively exclude them. Finally, when the whole FEI level reaches the set threshold, the final denoising signal can be obtained and shows obvious impulse features corresponding to fault feature frequency. It should be noted that although the proposed method has a good effect as a thought of signal decomposition and denoising, it still has some limitations. In the proposed method's application process, some parameters still need to be set, which is not a completely adaptive noise reduction process. Therefore, the adaptive adjustment of parameters is a key point of subsequent research. In addition, because the fault feature frequency components generated by different types of faults at the same location are similar, which may bring differences in amplitude and other aspects, the proposed method in this paper is mainly based on FEI value for component screening. Moreover, the accurate diagnosis methods for different types of faults at the same location need to be further studied.

5. Conclusions

The vibration signals of the gear contain strong noise and much interference, which affect the extraction of fault feature information. Therefore, a denoising method of vibration signals based on IMRSVD and effective component selection is proposed in this paper. In the proposed method, SVD is used to achieve the pre-decomposition and the reconstruction of the signal, and multiple one-dimensional components are obtained. Further decomposition and effective component selection are achieved by using IMRSVD and the proposed FEI index. The experiments were carried out by using a simulation signal and a real vibration signal of planetary gear, respectively. After processing the real vibration

signal by the proposed method, the FEI value of the normal gear increases from 0.028 to 0.048, and the FEI value of the gear with breakage is greatly improved from 0.034 to 0.125. That verified that the proposed denoising method could detect and retain fault feature information from noisy fault vibration signals, the noise interference and irrelevant components can be effectively eliminated, and the state of the gear can be judged according to the FEI value and spectrum analysis. In addition, the performance and difference between FEI and PMI are discussed, and the accuracy and robustness of FEI are demonstrated. Therefore, the proposed method is a reliable and effective tool for signal preprocessing and interference elimination.

Author Contributions: X.C. carried out the experimental analysis and wrote the manuscript; X.S. carried out the experimental analysis; C.L. carried out the experiment and analyzed the experimental data.; W.L. analyzed the experimental data. All authors have read and agreed to the published version of the manuscript.

Funding: This research was funded by the National Natural Science Foundation of China, grant number 51905147, the National Natural Science Foundation of Jiangsu Province, grant number BK20201163, Changzhou Sci & Tech Program, Grant number CJ20220208, and the Fundamental Research Funds for the Central Universities, grant number B210204005.

Data Availability Statement: The data used to support the findings of this study are available from the first author upon request.

Acknowledgments: The authors wish to thank the working reviewers and editors.

Conflicts of Interest: The authors declare no conflict of interest.

References

1. Kumar, A.; Gandhi, C.; Zhou, Y.; Kumar, R.; Xiang, J. Latest developments in gear defect diagnosis and prognosis: A review. *Measurement* **2020**, *158*, 107735. [CrossRef]
2. Chen, X.; Cheng, G.; Li, Y.; Peng, L. Fault diagnosis of planetary gear based on entropy feature fusion of DTCWT and OKFDA. *J. Vib. Control* **2017**, *24*, 5044–5061. [CrossRef]
3. Yang, J.; Wu, C.; Shan, Z.; Liu, H.; Yang, C. Extraction and enhancement of unknown bearing fault feature in the strong noise under variable speed condition. *Meas. Sci. Technol.* **2021**, *32*, 105021. [CrossRef]
4. Zhang, Q. and Liu, X. Optimization of the quality of the automatic transmission shift and the power transmission characteristics. *Energies* **2022**, *15*, 4672.
5. Mastrone, M.N.; Concli, F. A Multi Domain Modeling Approach for the CFD Simulation of Multi-Stage Gearboxes. *Energies* **2022**, *15*, 837. [CrossRef]
6. Bahri, M.; Amir, A.K.; Ashino, R. Linear canonical wavelet transform: Properties and inequalities. *Int. J. Wavelets, Multiresolution Inf. Process.* **2021**, *19*, 2150027. [CrossRef]
7. Jalayer, M.; Orsenigo, C.; Vercellis, C. Fault detection and diagnosis for rotating machinery: A model based on convolutional LSTM, Fast Fourier and continuous wavelet transforms. *Comput. Ind.* **2020**, *125*, 103378. [CrossRef]
8. Sharma, V.; Parey, A. Extraction of weak fault transients using variational mode decomposition for fault diagnosis of gearbox under varying speed. *Eng. Fail. Anal.* **2019**, *107*, 104204. [CrossRef]
9. Meng, F.; Xu, D.; Song, T. ATDNNS: An adaptive time–frequency decomposition neural network-based system for tropical cyclone wave height real-time forecasting. *Futur. Gener. Comput. Syst.* **2022**, *133*, 297–306. [CrossRef]
10. Lu, N.; Jiang, B.; Meng, X.; Zhao, H. Diagnosis, Diagnosticability Analysis, and Test Point Design for Multiple Faults Based on Multisignal Modeling and Blind Source Separation. *IEEE Trans. Syst. Man, Cybern. Syst.* **2017**, *50*, 137–148. [CrossRef]
11. Li, C.; Yu, G.; Fu, B.; Hu, H.; Zhu, X.; Zhu, Q. Fault Separation and Detection for Compound Bearing-Gear fault Condition Based on Decomposition of Marginal Hilbert Spectrum. *IEEE Access* **2019**, *7*, 110518–110530. [CrossRef]
12. Zhang, M.; Liang, K.; Miao, Y.; Lin, J.; Ding, C. Application of improved double-dictionary K-SVD for compound-fault diagnosis of rolling element bearings. *Measurement* **2021**, *187*, 110168. [CrossRef]
13. Wang, S.; Niu, P.; Guo, Y.; Wang, F.; Li, W.; Shi, H.; Han, S. Early diagnosis of bearing faults using decomposition and reconstruction stochastic resonance system. *Measurement* **2020**, *158*, 107709. [CrossRef]
14. Xiao, L.; Zhang, X.H.; Lu, S.L.; Xia, T.B.; Xi, L.F. A novel weak-fault detection technique for rolling element bearing based on vibrational resonance. *J. Sound Vib.* **2019**, *438*, 490–505. [CrossRef]
15. Wang, Z.; Zhou, J.; Du, W.; Lei, Y.; Wang, J. Bearing fault diagnosis method based on adaptive maximum cyclostationarity blind deconvolution. *Mech. Syst. Signal Process.* **2022**, *162*, 108018. [CrossRef]
16. Miao, Y.; Zhang, B.; Zhao, M.; Lin, J. Period-oriented multi-hierarchy deconvolution and its application for bearing fault diagnosis. *ISA Trans.* **2021**, *114*, 455–469. [CrossRef]

17. Osornio-Rios, R.A.; Jaen-Cuellar, A.Y.; Alvarado-Hernandez, A.I.; Zamudio-Ramirez, I.; Cruz-Albarran, I.A.; Antonino-Daviu, J.A. Fault detection and classification in kinematic chains by means of PCA extraction-reduction of features from thermographic images. *Measurement* **2022**, *197*, 111340.
18. Zamudio-Ramirez, I.; Saucedo-Dorantes, J.J.; Antonino-Daviu, J.; Osornio-Rios, R.A.; Dunai, L. Detection of Uniform Gearbox Wear in Induction Motors Based on the Analysis of Stray Flux Signals Through Statistical Time-Domain Features and Dimensionality Reduction Techniques. *IEEE Trans. Ind. Appl.* **2022**, *58*, 4648–4656. [CrossRef]
19. Hu, Y.; Tu, X.; Li, F.; Li, H.; Meng, G. An adaptive and tacholess order analysis method based on enhanced empirical wavelet transform for fault detection of bearings with varying speeds. *J. Sound Vib.* **2017**, *409*, 241–255. [CrossRef]
20. Xiao, Q.; Li, J.; Zeng, Z. A denoising scheme for DSPI phase based on improved variational mode decomposition. *Mech. Syst. Signal Process.* **2018**, *110*, 28–41. [CrossRef]
21. Hu, B.; Li, B. A new multiscale noise tuning stochastic resonance for enhanced fault diagnosis in wind turbine drivetrains. *Meas. Sci. Technol.* **2016**, *27*, 025017. [CrossRef]
22. Laha, S. Enhancement of fault diagnosis of rolling element bearing using maximum kurtosis fast nonlocal means denoising. *Measurement* **2017**, *100*, 157–163. [CrossRef]
23. Eltaieb, R.A.; Abouelela, H.A.E.; Saif, W.S.; Ragheb, A.; Farghal, A.E.A.; Ahmed, H.E.-D.H.; Alshebeili, S.; Shalaby, H.M.H.; El-Samie, F.E.A. Modulation format identification of optical signals: An approach based on singular value decomposition of Stokes space projections. *Appl. Opt.* **2020**, *59*, 5989–6004. [CrossRef] [PubMed]
24. Wang, F.; Deng, G.; Ma, L.; Liu, X.; Li, H. Convolutional Neural Network Based on Spiral Arrangement of Features and Its Application in Bearing Fault Diagnosis. *IEEE Access* **2019**, *7*, 64092–64100. [CrossRef]
25. Ye, W.; Li, S.; Zhao, X.; Abubakar, A.; Bermak, A. A K Times Singular Value Decomposition Based Image Denoising Algorithm for DoFP Polarization Image Sensors with Gaussian Noise. *IEEE Sensors J.* **2018**, *18*, 6138–6144. [CrossRef]
26. Yi, C.; Lv, Y.; Dang, Z.; Xiao, H.; Yu, X. Quaternion singular spectrum analysis using convex optimization and its application to fault diagnosis of rolling bearing. *Measurement* **2017**, *103*, 321–332. [CrossRef]
27. Zhao, M.; Jia, X. A novel strategy for signal denoising using reweighted SVD and its applications to weak fault feature enhancement of rotating machinery. *Mech. Syst. Signal Process.* **2017**, *94*, 129–147. [CrossRef]
28. Zeng, M.; Zhang, W.; Chen, Z. Group-Based K-SVD Denoising for Bearing Fault Diagnosis. *IEEE Sensors J.* **2019**, *19*, 6335–6343. [CrossRef]
29. Golafshan, R.; Sanliturk, K.Y. SVD and Hankel matrix based de-noising approach for ball bearing fault detection and its assessment using artificial faults. *Mech. Syst. Signal Process.* **2016**, *70–71*, 36–50. [CrossRef]
30. Yin, X.B.; Xu, Y.; Sheng, X.W.; Shen, Y. Signal denoising method using AIC-SVD and its application to micro-vibration in reaction wheels. *Sensors* **2020**, *19*, 5032. [CrossRef]
31. Xu, L.; Chatterton, S.; Pennacchi, P. Rolling element bearing diagnosis based on singular value decomposition and composite squared envelope spectrum. *Mech. Syst. Signal Process.* **2021**, *148*, 107174. [CrossRef]
32. Fu, Z.M.; Xu, X.; Pan, H.X.; Zhao, X.P.; Liang, H.Y. Early fault identification of Ammunition supply system based MRSVD and elman neural network. *Mach. Des. Res.* **2019**, *35*, 165–168.